



**HAL**  
open science

## Mechanical characterisation of human ascending aorta dissection

Valerie Deplano, Mourad Boufi, Vlad Gariboldi, Anderson Loundou, Xavier Benoit D'journo, Jennifer Cautela, Amina Djemli, Yves Alimi

► **To cite this version:**

Valerie Deplano, Mourad Boufi, Vlad Gariboldi, Anderson Loundou, Xavier Benoit D'journo, et al.. Mechanical characterisation of human ascending aorta dissection. *Journal of Biomechanics*, 2019, pp.138-146. 10.1016/j.jbiomech.2019.07.028 . hal-02268507

**HAL Id: hal-02268507**

**<https://hal.science/hal-02268507>**

Submitted on 25 May 2020

**HAL** is a multi-disciplinary open access archive for the deposit and dissemination of scientific research documents, whether they are published or not. The documents may come from teaching and research institutions in France or abroad, or from public or private research centers.

L'archive ouverte pluridisciplinaire **HAL**, est destinée au dépôt et à la diffusion de documents scientifiques de niveau recherche, publiés ou non, émanant des établissements d'enseignement et de recherche français ou étrangers, des laboratoires publics ou privés.

# Mechanical characterisation of human ascending aorta dissection

Valérie Deplano<sup>a,\*</sup>, Mourad Boufi<sup>b,a</sup>, Vlad Gariboldi<sup>c</sup>, Anderson D. Loundou<sup>d</sup>, Xavier Benoit D'Journo<sup>e</sup>, Jennifer Cautela<sup>f</sup>, Amina Djemli<sup>g</sup>, Yves S. Alimi<sup>b</sup>

<sup>a</sup>*Aix Marseille Univ, CNRS, IRPHE, Ecole Centrale Marseille, Marseille, France*

<sup>b</sup>*Aix Marseille Univ, APHM, IFSTTAR, LBA, North Hospital, Department of vascular surgery, Marseille, France*

<sup>c</sup>*Aix Marseille Univ, APHM, Timone Hospital, Department of cardiac surgery, Marseille, France*

<sup>d</sup>*Aix Marseille Univ, SPMC EA3279, Department of Public Health, Marseille, France*

<sup>e</sup>*Aix Marseille Univ, APHM, North Hospital, Department of thoracic surgery, Marseille, France*

<sup>f</sup>*Aix Marseille Univ, APHM, North Hospital, Department of cardiology, Marseille, France*

<sup>g</sup>*Aix Marseille Univ, APHM, North Hospital, Department of pathology, Marseille, France*

---

## Abstract

Mechanical characteristics of both the healthy ascending aorta and acute type A aortic dissection were investigated using *in vitro* biaxial tensile tests, *in vivo* measurements via transoesophageal echocardiography and histological characterisations. This combination of analysis at tissular, structural and microstructural levels highlighted the following: *i*) a linear mechanical response for the dissected intimomedial flap and, conversely, nonlinear behaviour for both healthy and dissected ascending aorta; all showed anisotropy; *ii*) a stiffer mechanical response in the longitudinal than in the circumferential direction for the healthy ascending aorta, consistent with the histological quantifica-

---

\*Corresponding author

*Email address:* `valerie.deplano@univ-amu.fr` (Valérie Deplano)

tion of collagen and elastin fibre density; *iii*) a link between dissection and ascending aorta stiffening, as revealed by biaxial tensile tests. This result was corroborated by *in vivo* measurements with stiffness index,  $\beta$ , and Peterson modulus,  $E_p$ , higher for patients with dissection than for control patients. It was consistent with histological analysis on dissected samples showing elastin fibre dislocations, reduced elastin density and increased collagen density. To our knowledge, this is the first study to report biaxial tensile tests on the dissected intimomedial flap and *in vivo* stiffness measurements of acute type A dissection in humans.

*Keywords:* Human ascending aorta, Acute type A dissection, Biaxial tensile test, *In vivo* measurements, Histological analysis

---

## 1. Introduction

2 An aortic dissection is a vascular pathology consisting in a tear of the  
3 aortic wall intima layer which can propagate downstream or/and upstream  
4 along the aorta, creating a false lumen through which blood flows. The Stan-  
5 ford classification divides aortic dissections into two types: type A when the  
6 initial tear is located along the ascending aorta and upstream of the left sub-  
7 clavian artery, and type B when the tear is located on the descending aorta.  
8 Acute type A dissection is characterised by rapidly developing severe com-  
9 plications such as aortic rupture, whereas chronic dissection is not diagnosed  
10 initially, being asymptomatic; patients remain stable. Acute type A dissec-  
11 tion has a short- and long-term spontaneous mortality of 70% (Golledge et  
12 al., 2008) and although its prognosis has been improved by surgical treat-

13 ment, post-operative mortality remains high. The tear initiates when the  
14 aortic wall can no longer bear the wall stress exerted. While some biax-  
15 ial tensile tests (Matsumoto et al. (2009), Haskett et al. (2010), Martin et  
16 al. (2011), Azadani et al. (2012), Kamenskiy et al. (2014)), or pressurised  
17 tests (Labrosse et al. (2009)) have been performed on healthy samples of  
18 human ascending aorta, there are few existing studies on dissected samples  
19 from acute type A dissection. To the authors' knowledge, only Babu et al.  
20 (2015) assessed mechanical properties of entire wall fragments from type A  
21 dissection. Studies using biaxial tensile or bulge inflation tests have gener-  
22 ally focused on ascending thoracic aortic aneurysms (ATAA) (Okamoto et al.  
23 (2002), Pham et al. (2013), Duprey et al. (2016)) rather than on dissection.  
24 Moreover, there have been few *in vivo* investigations of mechanical behaviour  
25 in dissections on the ascending aorta. Koullias et al. (2005) and Vitarelli et  
26 al. (2006) used echocardiography measurements to assess structural charac-  
27 teristics of ATAA and Marfan patients respectively. Shingu et al. (2009) were  
28 the only authors to use an echo-tracking system to obtain distensibility mea-  
29 surements, but on chronic dissection. Furthermore, the components of the  
30 extracellular matrix (ECM), their concentration and their organization are  
31 known to play an essential role in the mechanical behaviour of the human  
32 aorta (Tsamis et al., 2013). Today, there is greater emphasis on quanti-  
33 fying the arterial microstructure and microarchitecture using, for example,  
34 microscopy image analysis (Koch et al., 2014) to corroborate macroscopic  
35 mechanical response and enrich constitutive laws and thus numerical mod-  
36 elling (Pasta et al. (2014), Thunes et al. (2018)).

37 Here, we sought insights into the mechanical behaviour of the ascending

38 aorta in acute type A dissection because of its high mortality risk. Three me-  
39 chanical characterisations were therefore performed at different investigation  
40 levels. *In vivo* measurements were performed on both healthy and patholog-  
41 ical patients to obtain results at structure level. These measurements were  
42 combined with appropriate *in vitro* biaxial tensile tests on both healthy and  
43 dissected aortic samples to assess information at tissular level. Finally, qual-  
44 itative and quantitative histological analyses were carried out on both types  
45 of samples to link structural, tissular and microstructural level.

## 46 **2. Methods**

### 47 *2.1. Tissue preparation*

48 Healthy ascending aorta, *Haa*, tubular structures were harvested from un-  
49 used aortic segments after lung transplantation. Dissected ascending aorta,  
50 *Daa*, fragments were collected from patients after surgical repair. Informed  
51 consent was obtained based on established research board protocol in each  
52 hospital. All samples were stored, refrigerated at 4°C in 0.9% NaCl solution  
53 and tested less than 50h after tissue extraction.

54 The *Haa* tubular structures (figure 1a) were longitudinally cut along the  
55 curvature. Three types of samples were extracted from dissected fragments  
56 (figure 1b) : a region without dissected layers, *WDaaL*, n=1, (figure 1d),  
57 the adventitia layer alone, n=3, (figure 1e), and the media associated with  
58 the intima layer called intimomedial flap, n=3, (figure 1f). Square 20X20mm  
59 samples (a reproducible size) were subsequently obtained from healthy and  
60 dissected samples, using a dedicated cutting device. Seven healthy samples  
61 from 5 different donors of mean age  $65.3 \pm 4.9$  years, with a mean thickness

62 of  $2.26 \pm 0.19$ mm, were tested. The mean thickness and patient mean age  
63 of the flap and adventitia samples were  $1.98 \pm 0.12$ mm;  $63.7 \pm 9.2$  years and  
64  $1.06 \pm 0.17$ mm;  $59.7 \pm 8.3$  years respectively. The thickness of *WDaaL* was  
65 1.79mm and the patient was 57 years old. Thickness was measured via im-  
66 age processing of the undeformed samples (Deplano et al. (2016)). Table A.1  
67 Appendix A reported demographic data and risk factors of all *in vitro* tested  
68 samples.

69

## 70 2.2. *In vitro* mechanical tests

71 The square samples were mounted using a home-made biaxial set-up de-  
72 scribed in Deplano et al. (2016). Briefly, the circumferential,  $\theta$ , and longitu-  
73 dinal,  $L$ , directions of the sample were in line with the biaxial displacements.  
74 A displacement-driven protocol was applied while the ratio,  $\alpha$ , remained con-  
75 stant.  $\alpha = \frac{\lambda_\theta}{\lambda_L}$ , noted  $\alpha = \lambda_\theta : \lambda_L$ , was the stretch ratio,  $\lambda_\theta$  and  $\lambda_L$  being the  
76 stretch in the  $\theta$ , and  $L$  directions respectively.

77 Forces resulting from the displacements were measured using two load cells  
78 ( $10\text{N} \pm 0.0015\text{N}$ , 31E10, Honeywell) located on each direction of displace-  
79 ment. 3D displacement measurements (Dantec Q-400 software) were per-  
80 formed using Stereoscopic Digital Image Correlation. Samples were sub-  
81 merged in aqueous 0.9% NaCl solution maintained at  $37^\circ\text{C}$  during the ex-  
82 periments.

83 The maximum stretch,  $\lambda_{max}$ , was set at 1.2 of the gripped undeformed  
84 sample area,  $X_L \times X_\theta$ , where  $X_L = X_\theta = 18\text{mm}$  were measured before  
85 the protocol was applied. Twenty loading and unloading cycles of precon-  
86 ditioning were first performed at  $\lambda_{max}$  and  $\alpha = 1 : 1$  following by  $k=7$

87 consecutive cycles, each one at different stretch ratios : 0.75:1, 1:0.75, 0.5:1,  
88 1:0.5, 0.25:1, 1:0.25, 1:1. This protocol was applied for a maximum stretch  
89 rate of  $\lambda_{max} = 3.84 \times 10^{-2} s^{-1}$ . Initial zero stress was assessed by tuning  
90 the position of the suture lines by 0.1mm steps at a very low displacement  
91 rate (0.1mm/s) until the load cell signals detected were above their noise  
92 level (2.4mV). A hybrid displacement/force control was implemented during  
93 unloading to avoid bending the sample with respect to its original dimensions.

94  
95 The first Piola Kirchhoff stress tensor,  $P$ , was determined using  $f_\theta$  and  
96  $f_L$ , the recorded force,  $X_\theta^{k-1}$ ,  $X_L^{k-1}$  and  $E_0$ , the undeformed gripped sample  
97 dimensions and thickness. For each cycle performed during one protocol,  
98  $X_\theta^{k-1}$  and  $X_L^{k-1}$  correspond to the undeformed lengths of the sample at the  
99 end of the k-1 unloading path.

100 The components of  $P$  were expressed by  $P_{\theta\theta}^k = \frac{f_\theta}{X_L^{k-1} E_0}$  and  $P_{LL}^k = \frac{f_L}{X_\theta^{k-1} E_0}$ .  
101 The components of the second Piola Kirchhoff stress tensor,  $S$ , were then  
102 obtained using  $S_{\theta\theta}^k = \frac{P_{\theta\theta}^k}{\lambda_\theta}$  and  $S_{LL}^k = \frac{P_{LL}^k}{\lambda_L}$ , those of the Cauchy stress tensor,  
103  $\sigma$ , using:  $\sigma_{\theta\theta}^k = P_{\theta\theta}^k \lambda_\theta$  and  $\sigma_{LL}^k = P_{LL}^k \lambda_L$ .  $\lambda_i$  were calculated from the SDIC  
104 displacement measurements. The superscript  $k$  will be omitted in the rest of  
105 the paper.

### 107 2.3. Histological characterisation

108 Healthy and dissected segments (n=3 and n=4 respectively) were first  
109 fixed in 10% formalin (Appendix A details their characteristics). For each  
110 sample, 2 contiguous samples were cut along the axial and transversal artery  
111 axis. They were dehydrated in ethanol and embedded in paraffin. Four con-

112 tiguous sections 5  $\mu\text{m}$  thick were cut and stained with orceid and Trichrome  
113 masson for the visualisation of elastin and collagen fibres respectively. Calopix  
114 software was then used for image processing and extraction of the relative  
115 density of the stained structures. Density was defined as the ratio of stained  
116 surface to total surface for a region of interest of the sample. For each sam-  
117 ple, density was measured in 4 regions in media layers and in the entire wall,  
118 and averages were calculated.

#### 119 2.4. *In vivo* measurements

120 To determine the mechanical behaviour of both healthy and dissected  
121 ascending aorta, *in vivo* transoesophageal echocardiography measurements  
122 were performed on two new groups of patients not used for the *in vitro* tests  
123 and histological characterisations. The control group (n=22, age  $67\pm 9$  years,  
124 19 males) was composed of patients without any ascending aorta pathology,  
125 while the second group (n=13, age  $69\pm 10$  years, 9 males) was composed of  
126 patients admitted and treated for acute type A dissection. The mechanical  
127 characterisation of both groups entailed determining the Peterson modulus,  
128  $E_p$ , and stiffness index,  $\beta$ .  $E_p = \frac{\Delta P}{\epsilon}$ ,  $\beta = \frac{\ln \frac{P_{sys}}{P_{dias}}}{\epsilon}$ , where  $\epsilon = \frac{\Delta D}{D_{dias}}$ ,  $\Delta P$  and  
129  $\Delta D$  were the difference between the diastolic and systolic pressure ( $P_{dias}$ ,  
130  $P_{sys}$ ) and diameter ( $D_{dias}$ ,  $D_{sys}$ ) values respectively. Details of pressure and  
131 diameter acquisitions as well as inclusion criteria for each group are given in  
132 Appendix B.



### 133 3. Results

#### 134 3.1. Constitutive modelling

135 Figures 2a) to d), which represent  $S - \lambda$  curves for both  $Haa$  and  $WDaaL$   
136 samples, show nonlinear and rather anisotropic behaviour. These mechanical  
137 responses were therefore modelled by a Holzapfel-Gasser-Ogden (HGO) form  
138 of strain energy function,  $\psi$ , as per Babu et al. (2015).

139  $\psi = \psi_{iso} + \psi_{aniso}$  with  $\psi_{iso} = \frac{C}{2}(I_1 - 3)$  and  $\psi_{aniso} = \frac{k_1}{k_2}(e^{(k_2(I_4 - 1)^2)} - 1)$  consid-  
140 ering that collagen fibres are symmetrically oriented in the arterial wall.  $C$   
141 and  $k_1$  are positive dimensional (Pa) coefficients and  $k_2$  is dimensionless.  $I_1$   
142 is the first invariant of the strain tensor and  $I_4 = \lambda_\theta^2 \cos^2 \gamma + \lambda_L^2 \sin^2 \gamma$ , where  
143  $\gamma$  is the angle between the fibre direction and the circumferential direction.

144

145 Figures 3 a) and b), which show  $S - E$  curves for the  $Daa$  intimomedial  
146 flap, highlight more or less linear and anisotropic behaviour. According to  
147 these results, the mechanical response was described by a 3-parameter poly-  
148 nomial strain energy function,  $\psi = \frac{1}{2}(A_{\theta\theta}E_{\theta\theta}^2 + 2A_{\theta L}E_{\theta\theta}E_{LL} + A_{LL}E_{LL}^2)$ .  $E_{\theta\theta}$   
149 and  $E_{LL}$  are the components of the Green-Lagrangian strain tensor. The co-  
150 efficients  $A_{\theta\theta}$  and  $A_{LL}$  describe the tissue stiffness in the  $\theta$  and  $L$  directions  
151 respectively and  $A_{\theta L}$  is related to the interaction between the two directions.

152 Whatever the constitutive modelling, the components of the second Piola  
153 Kirchhoff stress tensor can be derived from  $\psi$  according to  $S = \frac{\partial \psi}{\partial E}$ . The  
154 coefficients  $C$ ,  $k_1$ ,  $k_2$  and  $\gamma$  angle for the HGO model, and  $A_{\theta\theta}$ ,  $A_{LL}$  and  
155  $A_{\theta L}$  for the linear model were thus obtained using an optimization procedure  
156 (using `fmincon` function in Matlab). Part of the mechanical data from the  
157 biaxial protocol was simultaneously fitted to the constitutive model. For

158 *Haa* and *WDaaL*, mechanical data from  $\alpha= 0.5:1; 1:0.5$ , and  $1:1$  were used.  
 159 For the *Daa* flap, mechanical data from  $\alpha= 0.75:1; 1:0.75, 0.5:1, 1:0.5$  were  
 160 considered.

161 The method involved minimizing the sum of the error  $\chi_\alpha$  (equation 1), e.g.  
 162  $\sum_\alpha \chi_\alpha$  where  $\alpha$  was the stretch ratio and  $m$  the number of experimental data  
 163 recorded during loading (e.g  $m=60$ ).

$$\chi_\alpha = \sum_{k=1}^m (S_{\theta\theta}^{exp} - S_{\theta\theta}^{mod})_k^2 + (S_{LL}^{exp} - S_{LL}^{mod})_k^2 \quad (1)$$

164 The superscript *exp* indicates the stress values from the experimental data,  
 165 *mod* those predicted by the model.

166 Table C.1 Appendix C displays the  $C$ ,  $k_1$ ,  $k_2$  coefficients and  $\gamma$  angle for  
 167 the mean data obtained from the healthy samples ( $n=7$ ) and for the single  
 168 *WDaaL* sample tested. Table C.2 Appendix C presents the  $A_{ij}$  coefficients  
 169 obtained through the optimization procedure for each *Daa* flap sample and  
 170 the mean data obtained from all flap samples. For each constitutive mod-  
 171 elling process, the coefficients obtained at the end of optimization procedures  
 172 converged towards the same values, whatever the initial guesses tested.

173

174 For mean data obtained from *Haa* samples and *WDaaL* data, the stress  
 175 components derived from the strain energy function fitted the experimental  
 176 data with average determination coefficients  $\overline{R_L^2}$  of 0.811 and 0.911 respec-  
 177 tively and  $\overline{R_\theta^2}$  of 0.861 and 0.902 respectively (Table C.1 Appendix C). For  
 178 mean data obtained from the flap samples, we found  $\overline{R^2}$  of 0.991 and 0.995  
 179 in the longitudinal and circumferential direction respectively (Table C.2 Ap-  
 180 pendix C). Figures 3a) and b) underline the good fit between experimental

181 data and constitutive modelling for flap mean data. This is further illustrated  
182 by figures 4a) and b), which show that the model's prediction of  $S - E$  be-  
183 haviour for  $\alpha = 1$  is very close to the experimental behaviour, even though  
184 this latter dataset was not used in the identification procedure.

### 185 *3.2. Mechanical behavior of healthy and dissected ascending aorta*

#### 186 *3.2.1. In vitro mechanical tests*

187 None of the tensile tests performed on the adventitia *Daa* samples could  
188 be exploited, due to systematic tearing under stress.

189 To compare the mechanical behaviour of *Haa* with that of *WDaaL*,  $\sigma$ - $\lambda$   
190 curves for  $\alpha=1$  in both longitudinal and circumferential directions were plot-  
191 ted using an HGO model (figure 5). As mentioned, both samples exhibited  
192 nonlinear and anisotropic behaviour. The mechanical response of *WDaaL*  
193 was stiffer than that of *Haa* and both their responses were stiffer in the  
194 longitudinal than in the circumferential direction. Although rather linear,  
195 the mechanical behaviour of *Daa* flap samples (figures 3a) and b) was also  
196 anisotropic ; however their  $A_{\theta\theta}$  coefficient was greater than  $A_{LL}$  one, 277.653  
197 versus 232.861 kPa, (Table C.2 Appendix C).

198 To compare anisotropy characteristics of *Haa* and *WDaaL*, stress levels  
199 at 80mmHg and 120mmHg were first computed using Laplace law  $\sigma_{\theta} = \frac{Pr}{h}$ ;  
200 P and r being  $P_{dias}$  and  $\frac{D_{dias}}{2}$  or  $P_{sys}$  and  $\frac{D_{sys}}{2}$  respectively (Table 2); h being  
201 the wall thickness. Using the experimental  $\sigma - \lambda$  curves, values of longitu-  
202 dinal and circumferential stretches were then inferred for  $\sigma_{\theta}$  Laplace values  
203 at 80 and 120mmHg using interpolation. The assessment of anisotropy at  
204 diastole,  $Ani_{80}$ , and systole,  $Ani_{120}$  were then defined (Kamenskiy et al.,  
205 2014) as the difference in longitudinal and circumferential stretches divided

206 by their average value. Whatever the stress level considered, the negative  
 207 anisotropy values confirm that mechanical response is stiffer in the longitu-  
 208 dinal direction for both healthy and *WDaaL* samples (Table C.1 Appendix  
 209 C). Moreover, these high values show that anisotropy increases when there  
 210 is dissection,  $Ani_{80}=-0.017$ ,  $Ani_{120}=-0.03$  for *Haa* versus -0.025 and -0.037  
 211 respectively for *WDaaL*. Finally, for *Daa* flap samples the mean anisotropic  
 212 level, defined as  $Ani = 2\frac{A_{LL}-A_{\theta\theta}}{A_{LL}+A_{\theta\theta}}$ , is 0.175 (Table C.2 Appendix C). While  
 213 *Haa* and *WDaaL* show a stiffer response in the longitudinal direction, flap  
 214 samples behave in the opposite way.

215

### 216 3.2.2. Histological characterisation

217 Figures 6 and 7 illustrate histological transversal and axial cuts of *Haa*  
 218 and *Daa* flap samples respectively. A sketch of both cuts (figure 6e) shows  
 219 that the transversal cut (TC) and axial cut (AC) generate faces that will  
 220 be stretched in the longitudinal and circumferential direction respectively.  
 221 Observations of the *Haa* TC reveal less elastin and more collagen fibres than  
 222 for the AC (figures 6a), b) and c), d) respectively). The fibre areal densities  
 223 (Table 1) quantitatively confirm these qualitative data. The ratio of collagen  
 224 to elastic areal density within the *Haa* TC total wall is greater than for AC,  
 225 3.61 versus 1.68.

226

227 Qualitative and quantitative comparison of histological cuts of *Haa* and  
 228 dissected samples (figures 6, 7 and table 1) highlights lower elastin fibre den-  
 229 sity and higher collagen fibre density for the dissected samples within the  
 230 AC of the media layer compared to healthy samples ( $20\pm 2$  versus  $30\pm 6$  and

fibres	Healthy samples n=3		Dissected samples n=4	
	Axial cut	Transversal cut	Axial cut	Transversal cut
<b>Within total wall</b>				
Elastin (%)	30±5.5	19.5±3	NA	NA
Collagen (%)	50.5±4	70.5±14	NA	NA
<b>Within media layer</b>				
Elastin (%)	30±6	18±2	20±2	24±3.5
Collagen (%)	54±4	66±8	60±4.5	45±6

Table 1: Average values in % of the elastin and collagen fibres areal density for both healthy and dissected samples.

231 60±4.5 versus 54±4 respectively). Moreover, figures 7b) and a) clearly show  
232 areas with broken elastin fibres and dislocations, when flap media are com-  
233 pared with *Haa* media.

234

### 235 3.2.3. *In vivo* measurements

236 Comparison of  $E_p$  and  $\beta$  parameters (Table 2) between the two groups of  
237 patients shows that those with dissection have a significantly higher stiffness  
238 index than control patients, with 20.7±24 versus 6.1±2.8, p=0.013. In addi-  
239 tion, mean  $E_p$  in the dissection group is 436±393 kPa, compared to 198±107  
240 kPa in the control group (p=0.041).

241 The systolic and diastolic aortic diameters are significantly larger in the  
242 dissection group (p<0.001 for both) and no correlation is found between sys-  
243 tolic ascending aorta diameter and stiffness index (p=0.87) and  $E_p$  (p= 0.82).

244

	Control group (n=22)	Dissection group (n=13)	p
Systolic diameter (mm)	34.8±4.9	47.7±5.5	<0.001
Diastolic diameter (mm)	33.4±4.9	44.3±5.2	<0.001
Systolic pressure (mmHg)	137±25	110±22	0.06
Diastolic pressure (mmHg)	79±14	57±17	0.01
$E_p$ (kPa)	198±107	436±393	0.041
$\beta$	6.1±2.8	20.7±24	0.013

Table 2: Systolic and diastolic diameter and pressure values from *in vivo* measurements. Resulting Peterson modulus and stiffness index values for control and dissection groups. Data were expressed as mean  $\pm$  standard deviation. Comparisons were performed using the Mann-Whitney U test. The statistical significance was defined as  $p < 0.05$

#### 245 4. Discussion and conclusion

246 The first question that merits discussion is whether the behaviour of the  
247 healthy aortic ascending wall is anisotropic or isotropic. This suggests the  
248 need to link analyses performed at different scales to enhance understanding.  
249 Results in the literature differ depending on the donors' age. Azadani et al.  
250 (2012) and Martin et al. (2011) showed isotropic behaviour for both relatively  
251 young (mean age 47) and very old (aged from 81 to 98) donors. Labrosse et  
252 al. (2009) and Haskett et al. (2010) observed anisotropic behaviour with a  
253 stiffer mechanical response in the circumferential direction than in the lon-  
254 gitudinal direction for patients aged from 31 to 71. However, Haskett et al.  
255 (2010) also observed that the longitudinal direction tended to stiffen with age  
256 more than the circumferential direction, with donors over 61 showing lower  
257 longitudinal than circumferential peak strain. In addition, Kamenskiy et al.  
258 (2014) reported that 7 patients out of 8, with a mean age of 54, had a more  
259 compliant mechanical response in the circumferential direction than longi-

260 tudinally. The general mechanical behaviour of our donors, 58 to 69 years  
261 old, nonlinear and anisotropic, is consistent with behaviours observed in the  
262 literature for the same age (figure 8). In our case, the mechanical response  
263 is stiffer in the longitudinal direction. In parallel, the ratio of collagen to  
264 elastic areal density is greater for a sample face stretched in the longitudinal  
265 direction. As collagen fibres contribute to stiffening whereas elastic fibres  
266 increase distensibility, the histological analysis confirms the results obtained  
267 using biaxial tensile tests.

268 Several components of the extra-cellular matrix may be involved in dissection  
269 and the associated mechanisms are not yet fully understood. Dysfunction in  
270 the contractile apparatus within smooth muscle cells may place the tho-  
271 racic aorta at increased risk (Emmott et al., 2016). Humphrey (2013) or  
272 Roccabianca et al. (2014) have, meanwhile, revealed that pooled glysamino-  
273 glycans/proteoglycans can induce stress concentration and pressure swelling  
274 within the aortic wall, and thus contribute to dissection. Nevertheless, elastin  
275 and collagen fibres are obviously implicated in arterial wall elasticity, tensile  
276 stiffness and strength, and anisotropy with stiffer mechanical response in the  
277 longitudinal direction could also play a role in dissection.

278 Few mechanical characterisations have been performed on dissected ascend-  
279 ing aortic walls; it is therefore important to compare healthy and dissected  
280 samples. Like *Haa*, *WdaaL* presents a stiffer mechanical response in the  
281 longitudinal direction. Although the number of samples we tested is a limi-  
282 tation, this result is in agreement with the only published work using biaxial  
283 tests to characterise the mechanical behaviour of *WDaaL*: Babu et al. (2015)  
284 observed the same anisotropic feature for patients over 50 years old with a

285 dissection. Complementarity between *in vitro* and *in vivo* measurements, a  
286 strength of our method, enables us to further the analysis. By subjecting  
287 excised aorta samples to mechanical solicitation via *in vitro* biaxial tensile  
288 tests, anisotropy, nonlinearity and stress are assessed at different stretch  
289 values; Young's modulus can also be inferred within a specific range of so-  
290 licitations. *In vivo* measurements enable aorta radial strain and pressure to  
291 be assessed at systolic and diastolic instants, thereby revealing aorta disten-  
292 sibility ( $\beta$  or  $E_p$ ). These two supplementary measurements allow arterial  
293 stiffness to be assessed from a different perspective. Here, *WDaaL* showed  
294 greater rigidity than *Haa*. Only one *WdaaL* was tested, but this *in vitro*  
295 assessment is confirmed by *in vivo* measurements performed on 13 patients  
296 with dissection and 22 without. Patients with dissection had a significantly  
297 higher stiffness index and  $E_p$  values than control. Moreover, as the *in vivo*  
298 measurements were performed on patients of comparable ages, the dissection  
299 stiffening cannot solely be associated with ageing. The relevance of our *in*  
300 *vivo* measurements is underlined by the fact that we found a mean  $E_p$  value  
301 in the control group, consistent with the literature values based on normal  
302 populations similar to ours in age and vascular risk factors (Hirata et al.  
303 (1991) and Stefanadis et al. (1990)).

304 Moreover, *in vivo* measurements can challenge assumptions in the clinical  
305 indexes used to evaluate dissection risk. The aortic diameter is often consid-  
306 ered an important parameter to assess dissection evolution. Here, although  
307 both systolic and diastolic diameters were significantly larger in the dissec-  
308 tion group, no correlation appears between systolic diameter and  $\beta$  or  $E_p$ . As  
309 dissection is clearly associated with stiffening, diameter does not therefore



310 appear to be relevant to predict the evolution of dissection.  
311 More work should be focused on better evaluating dissection evolution risk.  
312 Not only is there a lack of mechanical characterisations of dissected aorta  
313 samples, but there is also a pressing need to couple such studies with mi-  
314 crostructural analysis, so as to link overall mechanical response to microstruc-  
315 tural modification and focus on local changes in wall integrity.

316

317 Furthermore, fluid structure numerical modelling can add important in-  
318 formation on the quantification of hemodynamic loads at the wall and which  
319 are thus transmitted/perceived by the arterial wall cells. To date, few nu-  
320 merical studies have used FSI modelling and appropriate arterial wall consti-  
321 tutive laws (Alimohammadi et al., 2016). The results obtained in this work  
322 on flap and dissected ascending aorta wall stiffness could be used to perform  
323 such FSI numerical simulations, thereby contributing to the understanding  
324 of hemodynamic stimuli. This would improve modelling of the aortic cell  
325 response to such hemodynamic solicitations.

326

327 To conclude, this work used *in vitro* biaxial tensile tests, *in vivo* mea-  
328 surements via transoesophageal echocardiography and histological character-  
329 isation for ascending aorta mechanical characterisation, thereby combining  
330 tissular, structural and microstructural levels in an original approach. To  
331 our knowledge, this is the first study reporting biaxial tensile tests on the  
332 intimomedial flap, and our *in vivo* investigations of mechanical properties on  
333 acute type A dissection are the first in humans. Our major findings are : *i)*  
334 The mechanical response of the intimomedial flap shows linear behaviour up

335 to stretch values of 1.2. Conversely,  $Haa$  and  $WDaaL$  behave in a nonlinear  
336 way. However, all show anisotropy. *ii*) The mechanical response of  $Haa$  in  
337 the longitudinal direction is stiffer than in the circumferential direction. *iii*)  
338 Dissection promotes ascending aorta stiffening.

339

340 The present work has some limitations. A larger number of samples would  
341 be preferable, especially for biaxial tensile tests; we were mainly limited by  
342 the logistics of testing fresh tissue. The tensile test protocol was established  
343 in such a way as to be relevant to both healthy and dissected samples. In  
344 particular, a rather low value of  $\lambda_{max}=1.2$  was chosen to test the dissected  
345 adventitia layer because of its fragility. Unfortunately, we did not manage  
346 to test this specific sample, which would have permitted us to increase  $\lambda_{max}$   
347 for the other mechanical tests. Finally, the quantitative analysis of colla-  
348 gen results contained in the histomorphetric data should be considered with  
349 caution, because of the nonspecific nature of Trichrome Masson staining. De-  
350 spite these limitations, which are currently the subject of ongoing studies,  
351 our combination of *in vitro*, *in vivo* and histological results provides new  
352 insights into the mechanical characteristics associated with ascending aorta  
353 dissection.

## 354 **5. Acknowledgment**

355 The authors thank the Labex MEC ANR-11-LABX-0092 for financial  
356 support. We thank Marjorie Sweetko for English language revision.

### **Conflict of interest statement**

All authors declare that there are no conflict of interest.



## References

- Alimohammadi, M., Pichardo-Almarza, C., Agu, O., and Diaz-Zuccarini. V., 2016. Development of a patient-specific multi-scale model to understand atherosclerosis and calcification locations : comparison with *in vivo* data in aortic dissection. *Frontiers in Physiology, Computational Physiology and Medicine*, 7 :238.
- Azadani, A., Chitsaz, S., Matthews, P., Jaussaud, N., Leung, J., Tsinman, T., Ge, L., and Tseng, E., 2012. Comparison of Mechanical Properties of Human Ascending Aorta and Aortic Sinuses. *Ann Thorac Surg*, 93:87-94
- Babu, A.R., Byju, A.G., Gundiah, N., 2015. Biomechanical properties of human ascending thoracic aortic dissections. *Journal of biomechanical engineering*, 137/081013-1.
- Deplano, V., Boufi, M., Boiron, O., Guivier-Curien, C., Alimi, Y., Bertrand, E., 2016. Biaxial tensile tests of the porcine ascending aorta. *Journal of biomechanics*, 49(10), 2031-2037.
- Duprey, A., Trabelsi, O., Vola, M., Favre, JP., Avril, S., 2016. Biaxial rupture properties of ascending thoracic aortic aneurysms. *Acta Biomater.*, 15;42:273-285.
- Emmott, A., Garcia,J.,Chung, J., Lachapelle, K, El-Hamamsy,I., Mongrain, R., Cartier, R. and Leask, R.L. Biomechanics of the Ascending Thoracic Aorta: A Clinical Perspective on Engineering Data. *Canadian Journal of Cardiology*, 32(1),35-47.

- Golledge, J., Eagle, KA., 2008. Acute aortic dissection. *Lancet.*, 5; 372(9632).
- Haskett, D., Johnson, G., Zhou, A., Utzinger, U., Vande Geest, J., 2010. Microstructural and biomechanical alterations of the human aorta as a function of age and location. *Biomech Model Mechanobio.*, 9:725-736.
- Hirata, K., Triposkiadis, F., Sparks, E., Bowen, J., Wooley, C.F., Boudoulas, H., 1991. The Marfan syndrome: abnormal aortic elastic properties. *J Am Coll Cardiol.*, 18(1):57-63.
- Humphrey, J.D. 2013. Possible Mechanical Roles of Glycosaminoglycans in Thoracic Aortic Dissection and Associations with Dysregulated TGF- $\beta$ . *J Vasc Res.* 2013; 50(1): 110.
- Kamenskiy, A., Dzenis, Y., Jaffar Kazmi, S., Pemberton, M., Pipinos, I., Phillips, N., Herber, K., Woodford, T., Bowen, R., Lomneth, C., MacTaggart, J., 2014. Biaxial mechanical properties of the human thoracic and abdominal aorta, common carotid, subclavian, renal and common iliac arteries. *Biomech. Model Mechanobiol.*, 13:13411359
- Koch, R.G., Tsamis, A., D'Amore, A., Wagner, W.R., Watkins, S.C., Gleason, T.G., Vorp, D.A., 2014. A custom image-based analysis tool for quantifying elastin and collagen micro-architecture in the wall of the human aorta from multi-photon microscopy. *J. Biomech.*, 47, 935943.
- Koullias, G., Modak, R., Tranquilli, M., Korkolis, D., Barash, P., Elefteriades, J., 2005. Mechanical deterioration underlies malignant behavior of aneurysmal human ascending aorta. *J.Thorac Cardiovasc Surg.*, 130:677-83

- Labrosse, M.R., Beller, C.J., Mesana, T, Veiot, J.P., 2009. Mechanical behaviour of human aortas: experiments material constants and 3-D finite element modelling including residual stress. *Journal of biomechanics*, 42, 996-1004.
- Martin, C., Pham, T., Sun, W., 2011. Significant differences in the material properties between aged human and porcine aortic tissues. *European Journal of Cardio-thoracic Surgery.*, 40, 28-34.
- Matsumoto, T., Fukui, T., Tanaka, T., Ikuta, N., Ohashi, T., Kumagai, K., Akimoto, H., Tabayashi, K., Sato, M., 2009. Biaxial tensile properties of thoracic aortic aneurysm tissues. *J. Biomech. Sci. Eng.*, 4. 518-529
- Okamoto, R.J., Wagenseil, J.E., Delong, W.R., Peterson, S.J., Kouchoukos, N.T., Sundt, T.M., 2002. Mechanical properties of dilated human ascending aorta. *Annals of Biomedical Engineering*, 30, 624-635.
- Pasta, S., Phillippi, J.A., Tsamis, A., DAmore, A., Raffa, G.M., Pilato, M., Scardulla, C., Watkins, S.C., Wagner, W.R., Gleason, T.G., Vorp, D.A., 2016. Constitutive modelling of ascending thoracic aortic aneurysms using microstructural parameters. *Med. Eng. Phys.*, 38, 121130.
- Pham, T., Martin, C., Elefteriades, J., Sun, W., 2013. Biomechanical characterization of ascending aortic aneurysm with concomitant bicuspid aortic valve and bovine aortic arch. *Acta Biomater.*, 9(8):7927-36.
- Roccabianca, S., Figueroa, C.A., Tellides, G., Humphrey, J.D., 2014. Quantification of regional differences in aortic stiffness in the aging human. *Journal of the mechanical behavior of biomedical materials*, 29, 618-634.

- Roccabianca, S., Ateshian, G.A., Humphrey, J.D. 2017. Biomechanical roles of medial pooling of glycosaminoglycans in thoracic aortic dissection. *Biomech Model Mechanobiol.*, 13:1325.
- Shingu, Y., Shiiya, N., Ooka, T., Tachibana, T., Kubota, S., Morita, S., Matsui, Y., 2009. Augmentation index is elevated in aortic aneurysm and dissection. *Ann Thorac Surg.*, 87(5):1373-7.
- Stefanadis, C., Stratos, C., Boudoulas, H., Kourouklis, C., Toutouzas, P., 1990. Distensibility of the ascending aorta: comparison of invasive and non-invasive techniques in healthy men and in men with coronary artery disease. *Eur Heart J.*, 11(11):990-6.
- Thunes, J., Phillippi J, Gleason T, Vorp D, Maiti S., 2018. Structural modelling reveals microstructure-strength relationship for human ascending thoracic aorta. *Journal of Biomechanics*, 71, 8493
- Tsamis, A., Krawiec, J.T., Vorp, D.A., 2013. Elastin and collagen fibre microstructure of the human aorta in ageing and disease: a review. *Journal of the royal society interface*, 10:20121004.
- Vitarelli, A., Conde, Y., Cimino, E., D'Ángeli, I., D'Órazio, S., Stellato, S., Padella, V., Caranci, F., 2006. Aortic wall mechanics in the Marfan syndrome assessed by transesophageal tissue doppler echocardiography. *Am. J. Cardiol.*, 15;97(4):572-7

## Appendix A. Table of subject characteristics

Table A.1 details the subject characteristics of all the samples tested using the biaxial tensile set-up.

Donor(D)ID and Sample(S)ID	Age(yr)	Gender	Risk factors (Rf)
D1S1	69	M	HBP
D2S1, D2S2, D2S3	69	M	no Rf
D3S1	58	M	smoking
D4S1	59	F	no Rf
D5S1	64	M	HBP and smoking
Flap(F)ID and Sample(S)ID	Age(yr)	Gender	Risk factors
F1S1, F1S2	69	M	HBP
F2S1	53	M	no Rf
WDaaL(W)ID and Sample(S)ID	Age(yr)	Gender	Risk factors
W1S1	57	M	HBP

Table A.1: Donors and dissected subject characteristics. M for male, F for female, HBP for High Blood Pressure.

The number of healthy samples (n=3) histologically characterised, was a subset of those tested on the biaxial tensile device. Two out of four dissected samples, which have been histologically characterised, were also tested on the biaxial tensile device. The 2 dissected samples, that were not tested *in vitro*, came from patients with similar risk factors as those tested.



## Appendix B. Methodology of *in vivo* measurements

To determine the ascending aorta Peterson modulus and stiffness index for healthy and pathological cases, a standardized protocol using available TEE system (Philips EPIQ7 Ultrasound) with 4-7 MHz multiplane transoesophageal probe was used. Aortic diameters were measured 3 cm above the aortic valve location. Systole was detected by the full opening of aortic valve and end-diastole by the QRS wave peak on the simultaneously registered electrocardiogram. Pressure measurements were performed by sphygmomanometer for the control group and invasively by radial artery cannulation for the dissection group. A mean of two pressure measurements was retained for each patient. The dissection group was composed of patients aged from 50 to 85 years, with aortic dissection involving ascending aorta independently of the entry tear location occurring less than 2 weeks after the onset of symptoms. It is important to note that aortic dissection related to connective tissue genetic disorder (Marfan's or Ehlers-Danlos syndromes), iatrogenic dissection, type A intramural hematoma or dissection occurring in patients with bicuspid aortic valve were excluded of this pathological group. In the control group, patients were selected to match those in dissection group for age and vascular risk factors. They displayed no severe ascending aorta atherosclerosis, aortic-valve disease nor ascending aorta aneurysm.

### Appendix C. Tables of results: coefficients of constitutive modelling, $\overline{R^2}$ and anisotropy levels

Table C.1 shows  $C$ ,  $k_1$ ,  $k_2$  coefficients and  $\gamma$  angle for the mean data obtained from the healthy samples (n=7),  $\overline{Haa}$ , and for the only one tested sample of  $Daa$  wall without dissected layers.  $\overline{R^2}$  values obtained during the identification procedure and anisotropy level are also displayed.  $Ani_{80} = 2 \frac{\lambda_L^{80} - \lambda_\theta^{80}}{\lambda_L^{80} + \lambda_\theta^{80}}$  and  $Ani_{120} = 2 \frac{\lambda_L^{120} - \lambda_\theta^{120}}{\lambda_L^{120} + \lambda_\theta^{120}}$

	$C$ (kPa)	$k_1$ (kPa)	$k_2$	$\gamma$	$\overline{R_\theta^2}$	$\overline{R_L^2}$	$Ani_{80}$	$Ani_{120}$
$\overline{Haa}$	29.828	10.369	20.93	0.922	0.861	0.811	-0.017	-0.03
$Daa$ wall	13.950	62.056	12.01	0.879	0.902	0.911	-0.025	-0.037

Table C.1: Coefficients of the HGO constitutive modelling,  $\overline{R^2}$  values and anisotropy level obtained through the optimization procedure for  $\overline{Haa}$ , mean data obtained from the n=7 healthy samples and for  $Daa$  wall without dissected layers.

Table C.2 shows the  $A_{ij}$  constitutive modelling coefficients of  $Daa$  flap samples, the  $\overline{R^2}$  values obtained during the identification procedure and the anisotropy level,  $Ani = 2 \frac{A_{LL} - A_{\theta\theta}}{A_{LL} + A_{\theta\theta}}$ .

Flap(F)ID Sample(S)ID	$A_{\theta\theta}$ (kPa)	$A_{\theta L}$ (kPa)	$A_{LL}$ (kPa)	$\overline{R_\theta^2}$	$\overline{R_L^2}$	$Ani$
F1S1	299.375	111.499	251.451	0.988	0.992	0.174
F1S2	265.494	96.506	212.808	0.978	0.991	0.220
F2S1	293.325	114.408	236.580	0.980	0.976	0.214
Mean data	277.653	114.350	232.861	0.995	0.991	0.175

Table C.2:  $A_{ij}$  coefficients, anisotropy index and  $\overline{R^2}$  values obtained through the optimization procedure for each flap sample and for their mean data.

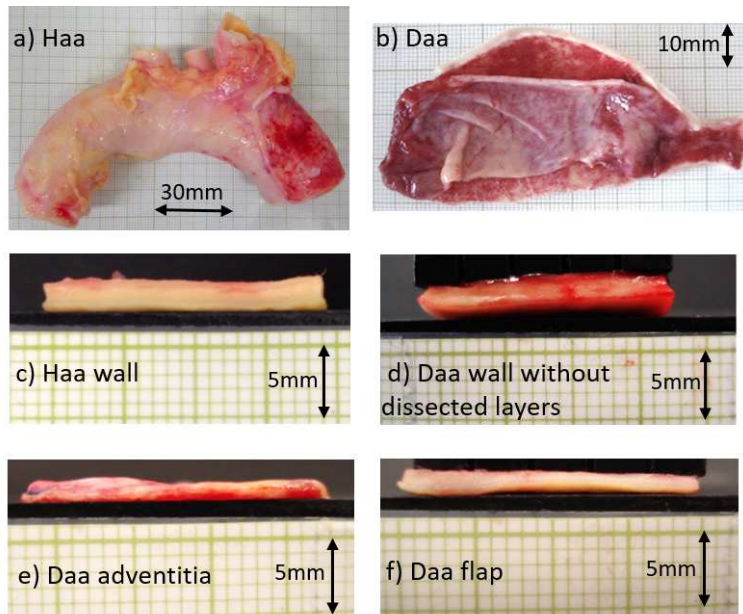


Figure 1: a) Representative healthy human ascending aorta, *Haa*. b) Representative fragment of dissected aorta, *Daa*. Side view of representative wall thickness of c) *Haa*, d) *Daa* without dissected layers, e) adventitia layer of *Daa*, f) intimomedial flap of *Daa*.

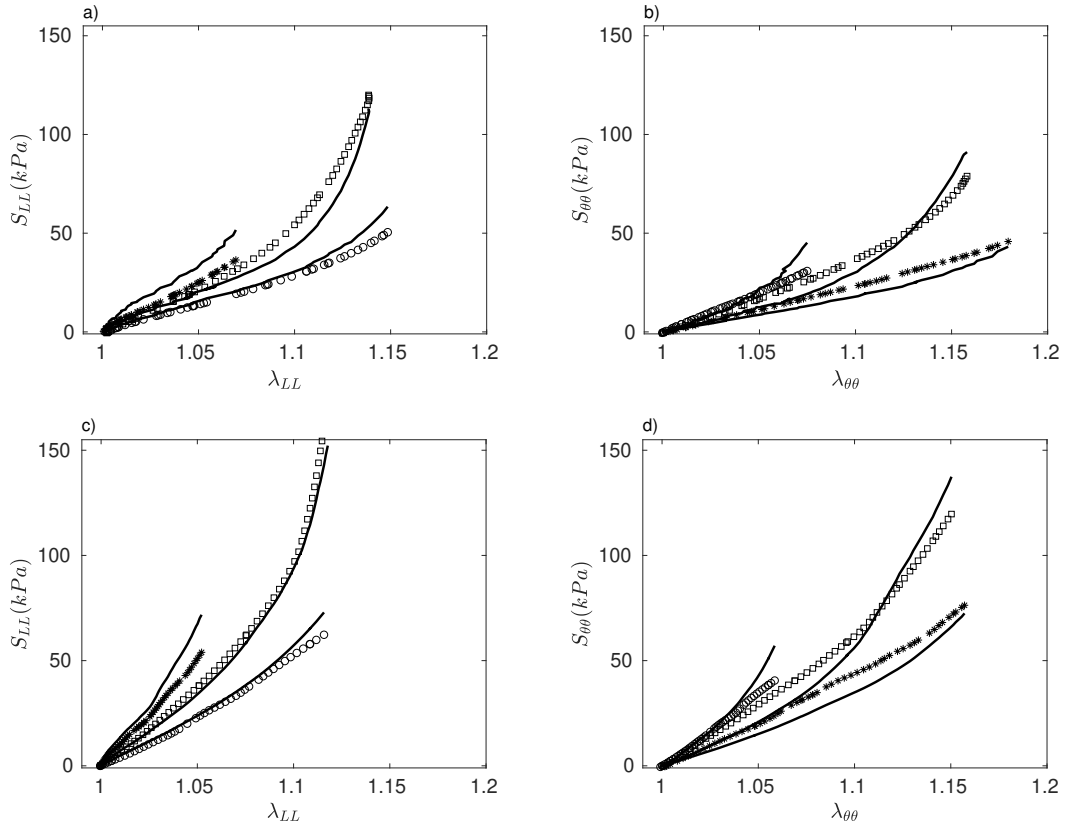


Figure 2: S- $\lambda$  curves. a) & b) Mean data obtained from *Haa* samples. c) & d) *Daa* wall without dissected layers.  $\alpha=0.5$  (circle symbol),  $\alpha=2$  (star symbol) and  $\alpha=1$  (square symbol). Symbols are used for experimental data and solid lines for constitutive modelling. a) and c): *L* direction. b) and d):  $\theta$  direction

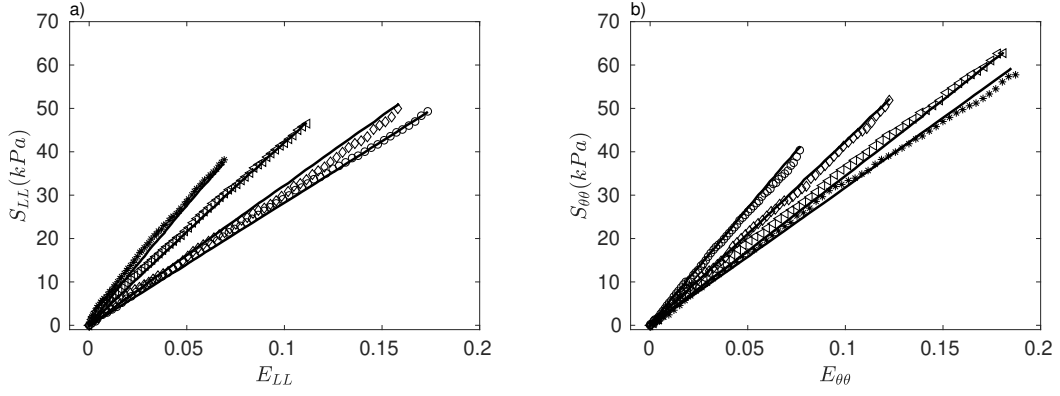


Figure 3: S-E curves plotted for the mean data obtained from the *Daa* intimomedial flap samples.  $\alpha=0.75, 1.33, 0.5,$  and  $2$  (diamond, triangle, circle and star symbols respectively). Symbols are used for experimental data and solid lines for constitutive modelling. a)  $L$  direction. b)  $\theta$  direction

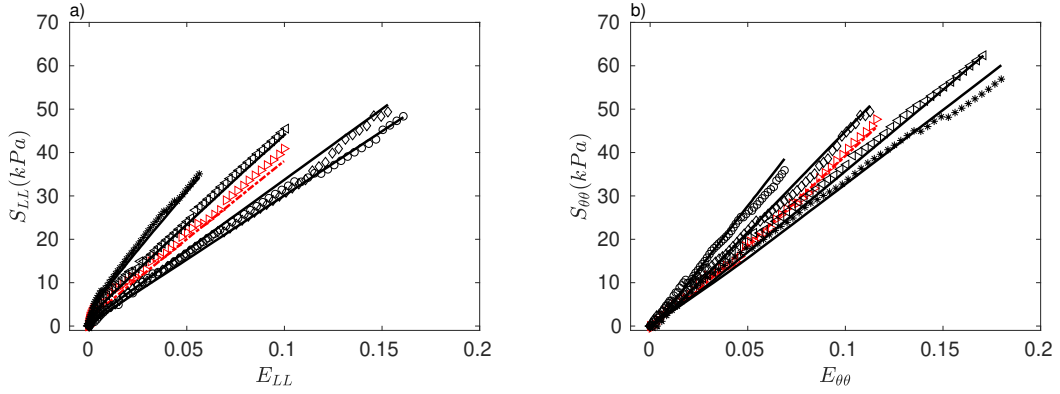


Figure 4: S-E curves illustrating a *Daa* intimomedial flap sample for  $\alpha=0.75, 1.33, 0.5,$  and  $2$  (diamond, triangle, circle and star symbols respectively). Symbols are used for experimental data and solid lines for constitutive modelling. Red curves are for  $\alpha=1$  that were not used for parameters identification. a)  $L$  direction. b)  $\theta$  direction

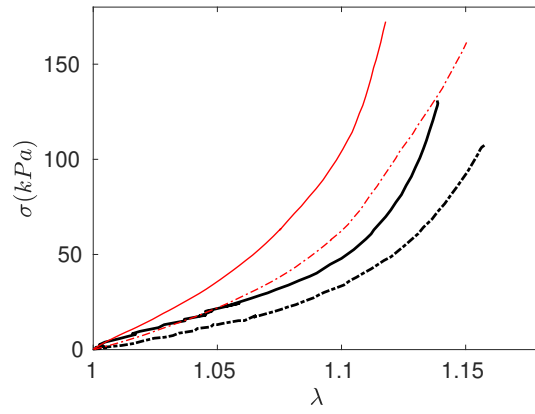


Figure 5: Comparison of  $\sigma - \lambda$  curves between *Daa* wall without dissected layers sample and *Haa* mean sample (red thin and black thick lines respectively). Curves are plotted using constitutive modelling and  $\alpha=1$ . Solid and dashed lines are used for the  $L$  and  $\theta$  direction respectively.

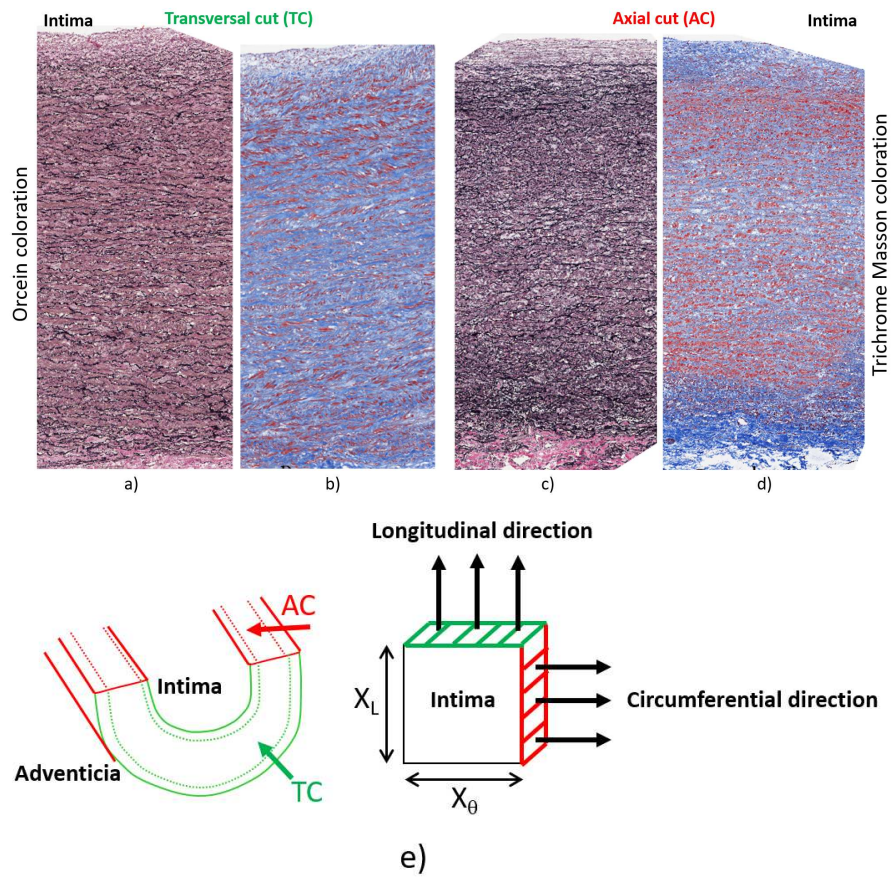


Figure 6: Transversal (a and b) and axial (c and d) histological cuts of *Haa*. Elastin fibres are colored in black a) and c) (orceid staining). Collagen fibres are colored in blue b) and d) (Trichrome masson staining). e) Scheme of arterial cuts and their corresponding stretching directions.



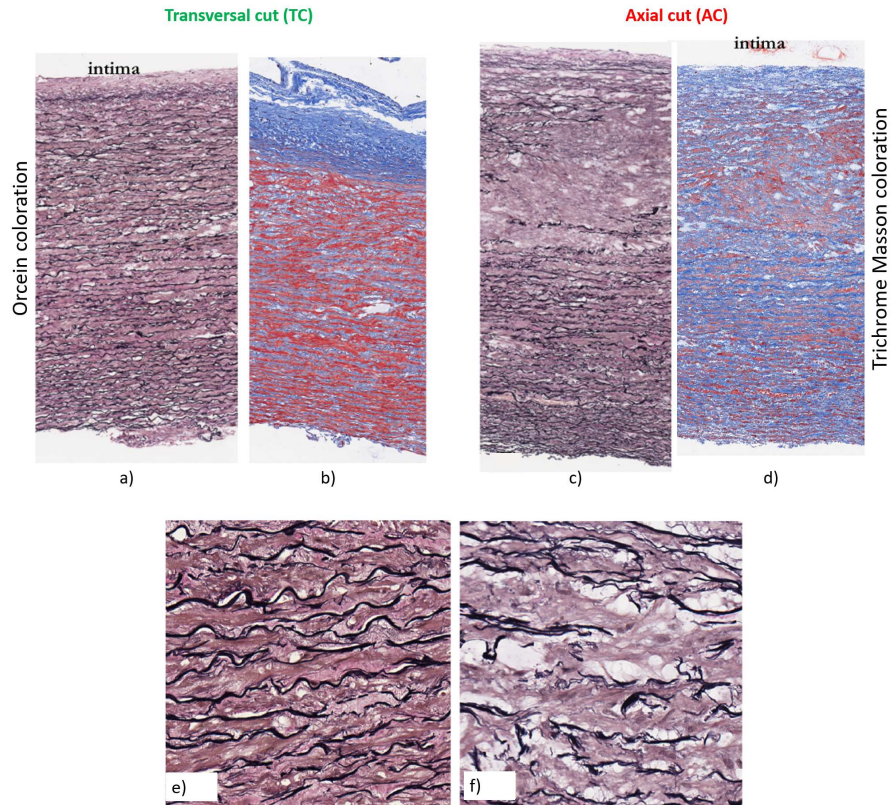


Figure 7: Transversal and axial histological cuts of *Daa* flap. Elastin fibres are colored in black a) and c) (orceid staining). Collagen fibres are colored in blue b) and d) (Trichrome masson staining). Zoom of the media layer histological transversal cut stained with orceid. e) Haa, f) Daa flap.



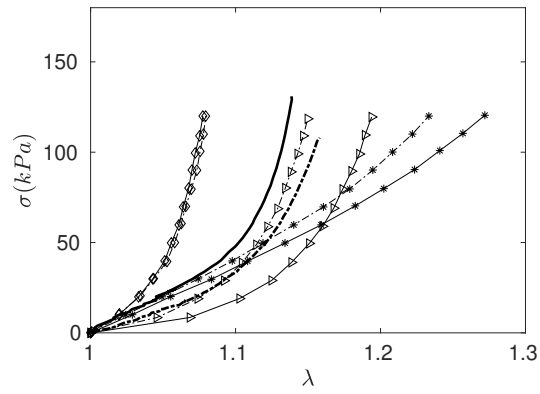


Figure 8: Comparison of  $\sigma - \lambda$  curves between mean values of our  $Haa$  samples (without symbol) and  $Haa$  of literature (diamond, triangle and star symbols for Martin et al. (2011) Labrosse et al. (2009) and Haskett et al. (2010) respectively; extracted from (Roccabianca et al., 2014)). Our curves are plotted using constitutive modelling and  $\alpha=1$ . Solid and dashed lines are used for the  $L$  and  $\theta$  direction respectively.